Naval Research Laboratory

Washington, DC 20375-5000

NRL Memorandum Report 6625

Millimeter-Wave Gyroklystron Amplifier Experiment Using A Relativistic Electron Beam

S. H. GOLD, A. W. FLIFLET, W. M. MANHEIMER,
D. A. KIRKPATRICK,* W. M. BLACK, A. K. KINKEAD,
D. L. HARDESTY, AND M. SUCY**

Beam Physics Branch
Plasma Physics Division

**Science Applications International Corporation, McLean, VA 22102*

***JAYCOR, Inc., Vienna, VA 22180*

March 8, 1990

UNCLASSIFIED
SECURITY CLASSIFICATION OF THIS PAGE

REPORT DOCUMENTATION PAGE

1a. REPORT SECURITY CLASSIFICATION Unclassified	1b. RESTRICTIVE MARKINGS
2a. SECURITY CLASSIFICATION AUTHORITY	3. DISTRIBUTION / AVAILABILITY OF REPORT Approved for public release; distribution unlimited.
2b. DECLASSIFICATION / DOWNGRADING SCHEDULE	
4. PERFORMING ORGANIZATION REPORT NUMBER(S) NRL Memorandum Report 6625	5. MONITORING ORGANIZATION REPORT NUMBER(S)
6a. NAME OF PERFORMING ORGANIZATION Naval Research Laboratory 6b. OFFICE SYMBOL (*If applicable*) Code 4793	7a. NAME OF MONITORING ORGANIZATION
6c. ADDRESS (*City, State, and ZIP Code*) Naval Research Laboratory Washington, DC 20375-5000	7b. ADDRESS (*City, State, and ZIP Code*)
8a. NAME OF FUNDING / SPONSORING ORGANIZATION Office of Naval Research 8b. OFFICE SYMBOL (*If applicable*)	9. PROCUREMENT INSTRUMENT IDENTIFICATION NUMBER 47-2797-0-0
8c. ADDRESS (*City, State, and ZIP Code*) ONR Arlingon, VA 22217	10. SOURCE OF FUNDING NUMBERS PROGRAM ELEMENT NO. / PROJECT NO. / TASK NO. RR011-09-4J / WORK UNIT ACCESSION NO.

11. TITLE (*Include Security Classification*)
Millimeter-Wave Gyroklystron Amplifier Experiment Using a Relativistic Electron Beam

12. PERSONAL AUTHOR(S) Gold, S.H., Fliflet, A.W., Manheimer, W.M., Kirkpatrick, D.A.*, Black, W.M., Kinkead, A.K., Hardesty, D.L., and Sucy, M.**

13a. TYPE OF REPORT	13b. TIME COVERED	14. DATE OF REPORT (*Year, Month, Day*)	15. PAGE COUNT
Memorandum	FROM 9/88 TO 3/90	1990 March 8	32

16. SUPPLEMENTARY NOTATION
*Science Applications International Corporation, McLean, VA 22102
**JAYCOR, Inc., Vienna, VA 22180

17. COSATI CODES			18. SUBJECT TERMS (*Continue on reverse if necessary and identify by block number*)
FIELD	GROUP	SUB-GROUP	Gyrotron; Gyroklystron; Millimeter-Wave; Relativistic Beam

19. ABSTRACT (*Continue on reverse if necessary and identify by block number*)

A fundamental mode TE^{o}_{111} two-cavity intense-beam gyroklystron amplifier experiment, operating at an accelerating voltage of 1 MV, has demonstrated a linear gain of 19 dB and an unsaturated power of 100 kW. The frequency of the second cavity has been found to track the frequency of the driven cavity over a range of 300 MHz around a center frequency of 35 GHz. Stable amplifier operation was achieved with beam currents as large as 150 A and a velocity pitch ratio of 0.36. The stable operating range was limited by spurious oscillation in the TE^{o}_{112} mode. Theoretical calculations indicate that higher gains might be attainable if this mode could be suppressed. The two cavities which were tested are intended to serve as bunching cavities for a high power output cavity to be tested at a later date.

20. DISTRIBUTION / AVAILABILITY OF ABSTRACT	21. ABSTRACT SECURITY CLASSIFICATION
☒ UNCLASSIFIED/UNLIMITED ☐ SAME AS RPT. ☐ DTIC USERS	Unclassified
22a. NAME OF RESPONSIBLE INDIVIDUAL S.H. Gold	22b. TELEPHONE (*Include Area Code*) 202-767-4004 / 22c. OFFICE SYMBOL Code 4793

DD FORM 1473, 84 MAR — 83 APR edition may be used until exhausted. All other editions are obsolete.

SECURITY CLASSIFICATION OF THIS PAGE
UNCLASSIFIED

CONTENTS

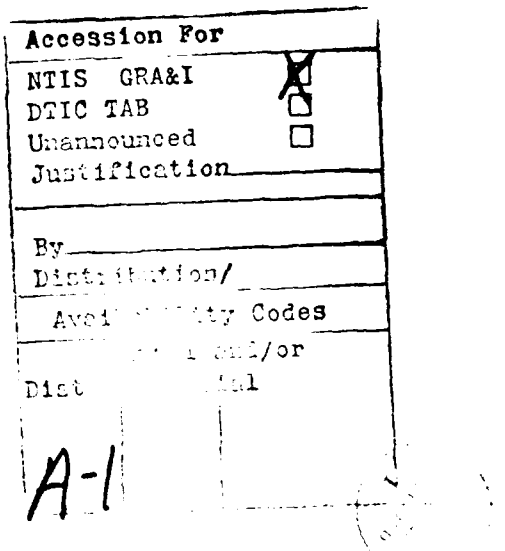

MILLIMETER-WAVE GYROKLYSTRON AMPLIFIER EXPERIMENT USING A RELATIVISTIC ELECTRON BEAM

I. Introduction

The gyrotron oscillator has proved to be a highly efficient source of high power millimeter–wave radiation. Much of the research on gyrotron oscillators has been motivated by the need to develop sources for cyclotron resonance heating of fusion plasmas [1]. However, there are a variety of applications in which the requirements for frequency and phase control are more demanding than for the fusion application. An example of this is the requirements imposed on the driver tubes for high power linear electron or positron accelerators, in which a large number of separate microwave sources must be in close phase synchronism to properly drive a long chain of acceleration cavities [2]. Another example is the requirements imposed on separate sources which will be combined for high power directed energy applications, such as when each source drives a separate element of a phased array antenna. For such applications, the gyroklystron amplifier has a number of natural advantages over the single–cavity gyrotron oscillator. With an amplifier, the required phase and frequency coherence should be attainable, and in addition, because of the possibility of controlling beam prebunching before entry into the final cavity where microwave power is produced, higher efficiency operation should be possible. Furthermore, by using multiple gyroklystron cavities, higher stable gain should be achievable than in gyro–traveling–wave amplifiers [see Ref. 3, and references therein].

A number of previous gyroklystron amplifier experiments have been reported in the literature. Symons and Jory [4] discuss a 50 kW, 28 GHz gyroklystron with 40 dB gain that employed a circular TE_{011} input cavity and a TE_{021} output cavity. It operated at 80 kV with an 8 A beam current, and achieved a saturated efficiency near 10%.

Manuscript approved March 19, 1990.

Significant difficulty was reported in this device with spurious oscillations in the input cavity and beam tunnel. This oscillation was suppressed by resistive loading of the undesired modes. Symons and Jory also report a second harmonic gyroklystron experiment, operating at 50 kV and 5 A, that produced 20 kW at 10.4 GHz. This device also experienced significant problems with oscillation in spurious modes. More recently, Bollen *et al.* [5] have reported a 50 kW, 4.5 GHz three–cavity gyroklystron amplifier operating at 35 kV and 5–10 A in a rectangular TE_{101} mode that achieved 30% efficiency. This device avoided mode competition by operating in the fundamental mode of rectangular cavities, with drift spaces that were cut off at the operating frequency.

In recent years, gyrotron oscillator operation has been extended to very high peak power (hundreds of megawatts) by employing high voltage ($\geq$ 1 MeV) intense ($\geq$ 1 kA) relativistic electron beams from pulseline accelerators [6]. There has been no corresponding extension reported for gyroklystron amplifiers. This paper reports the results of an initial experimental study of the operation of a two–cavity gyroklystron amplifier with fundamental mode cylindrical cavities operating near 1 MeV at relatively low current ($\geq$ 100 A). The two cavities were designed to serve as the bunching cavities for a higher power final output stage, to be implemented at a later date [7]. This study was intended to test the stability of the bunching cavities, and to demonstrate linear amplification of the drive signal. It was carried out at 35 GHz using a 50 nsec beam from a pulseline accelerator.

II. Apparatus

These experiments were carried out on the VEBA pulseline accelerator [8]. Figure 1 shows a schematic diagram of the experiment. An 8–mm–diam. solid electron beam was produced by an apertured diode that made use of beam scraping to produce a low–velocity spread beam with low initial transverse momentum [9]. The

diode operated in a uniform axial magnetic field of ~7.8 kG. The transverse momentum required for the gyrotron interaction was induced by transit through a one–period untapered bifilar helical wiggler magnet with 4–cm length, followed by adiabatic compression of the beam by means of a rise in the axial magnetic field to a final value of ~25 kG. After compression, the beam was designed to overfill the 4.32–mm–diam. beam tunnel leading to the first cavity, in order to correct for the decentering induced by passage through the wiggler magnet. The excess current is deposited on the walls of a graphite down–taper. The final beam current was monitored by a Rogowski coil at the entrance to the beam tunnel. The final axial magnetic field needed for the device was determined by the resonance condition for the first harmonic cyclotron maser interaction in the cavities, while the field in the vicinity of the wiggler magnet was chosen somewhat above the gyroresonant value [10]. This was done to produce the required beam α, where $\alpha = v_\perp/v_\parallel$ is the ratio of transverse to axial velocity, without inducing large momentum spread, which would be deleterious to operation of the gyroklystron.

The gyroklystron has two slotted cylindrical TE_{111} bunching cavities of identical design (but slightly different cold test properties), separated by a 4–cm–long drift space. Following the second cavity, an additional drift space leads to a TE_{121} slotted output cavity. Each cavity has a separate vacuum enclosure lined with microwave absorbing material, so that energy leakage from the slots will not couple back to the slots, or to another cavity. The bunching cavities can be accessed through the coupling apertures, which are labeled in Fig. 1 as **IN–1** and **IN–2**, respectively, and through the sampling apertures, labeled **OUT–1** and **OUT–2**. Figure 2 shows the details of the bunching cavity design, including the location of these apertures and of the slots used to control oscillation and mode competition. Figure 2 also shows the calculated axial rf–field profile for the TE_{111} and TE_{112} modes of the bunching cavities. The bunching cavity diameter is 5.7 mm, the nominal cavity length (not including field

penetration into the drift spaces) is 7.5 mm, and the drift space diameter is 4.32 mm. The present work deals only with the operation of the bunching cavities.

The bunching cavities were designed to operate at a total Q of 200, where Q is the cavity quality factor. The Q of each bunching cavity is given by

$$Q^{-1} = Q_{int}^{-1} + Q_{ext}^{-1} , \tag{1}$$

where Q_{int} is the internal cavity quality factor, determined principally by slot and ohmic losses, and Q_{ext} is the quality factor determined solely by losses through the cavity coupling aperture. It is convenient to define the coupling β as $\beta \equiv Q_{int}/Q_{ext}$. In terms of this parameter, the fraction $\mathcal{R}$ of incident power reflected from the coupling aperture at resonance is given by [11]:

$$\mathcal{R} = \frac{(1-\beta)^2}{(1+\beta)^2} \tag{2}$$

A value of β less than one is considered *undercoupled*, while a value greater than one is considered *overcoupled*. *Critical coupling* is defined as a coupling β of 1, a condition for which $\mathcal{R}$ goes to zero. For $\beta \sim 1$, a drive signal in the coupling arm should couple almost completely into the cavity.

The bunching cavity design called for $\beta \sim 1$, i.e., $Q_{int} \sim Q_{ext} \sim 400$. A pair of opposing axial slots, each of 44° transverse extent, was used to lower Q_{int} to 400 for the TE_{111} mode, while assisting in suppressing other competing modes [7]. The length of these slots is three times the nominal cavity length [see Fig. 2], in order to extend everywhere that the TE_{111} mode has substantial rf fields. The ohmic Q of the cavities is high compared to the Q associated with the slots, and may be neglected.

The presence of these slots also permit tuning of the resonant frequency of each cavity (to slightly higher frequencies) by transverse compression of the cavities.

The coupling apertures were designed to approximate critical coupling to the cavity (i.e., $Q_{ext} \sim 400$), while the sampling apertures were designed so as not to significantly load the cavities. For a particular (measured) reflected signal, Eq. (2) can be used to calculate two possible values for β which are reciprocals of each other. However, the measurement does not indicate which of these is the correct value. The remaining uncertainty can be resolved by slotted line measurements of the phase of the standing wave in the coupling arm. The procedure used to ensure nearly critical coupling began before the final cavity brazing took place. Each cavity was initially cold–tested with a very small coupling aperture ($\beta<<1$). The cavity Q–value and reflected signal were then determined, and the coupling aperture progressively enlarged, until the Q dropped by approximately a factor of two and the reflected signal at resonance dropped to near zero. At the conclusion of this process, each bunching cavity demonstrated a resonance within a few tens of MHz of 35 GHz accompanied by a large (~20 dB) dip in the reflected signal at resonance. At this point, the final cavity brazing was performed. The cold tests were then reverified, yielding center frequencies of 35.030 and 34.896 GHz for the first and second cavities, respectively. (The absolute accuracy of these two frequencies is ~0.1 %, or ±35 MHz, but the precision is ~1 MHz, which permits an accurate determination of the frequency difference between the cavities.) This frequency difference would correspond to a 7 μm difference in the diameter of the two cavities. In addition, the coupling to each cavity was nearly critical.

The desired operating frequency of the gyroklystron was 35.06 GHz (based on the calculated operating frequency of the TE_{121} output cavity). Each bunching cavity was then tuned to this frequency by tranverse compression by means of separate clamps. However, cavity deformation affects both the center frequency and the value

of Q. Following the tuning process, the approximate quality factors of the two cavities (the average of measurements performed driving the large and small apertures) were Q_1=230 and Q_2=140. The lower Q–value for the second cavity resulted from the greater amount of compression needed to tune this cavity to the desired frequency. At the final cavity tunings, the dip in the reflected signal for the first cavity was 18.6 dB, while the dip in the reflected signal for the second cavity was 11.6 dB. Based on the slotted–line measurements, each of the cavities was undercoupled. Hence, the value of β for the first cavity was 0.79, and for the second cavity was 0.58. For the first cavity, this means that the internal quality factor was 410. For the second cavity, this means that only ~37% of the power generated in the cavity would escape from IN–2.

As in previous gyroklystron devices, a critical design consideration was to avoid oscillation in either the operating mode of the bunching cavity or in other spurious modes. Oscillation in the design mode was avoided through control of the cavity Q–values by means of slot and aperture loading. Since the two bunching cavities were designed to operate in the fundamental TE_{11} mode of cylindrical cavities, no mode competition was possible from higher order transverse modes in first harmonic. The cavities were also designed for stability in higher–order transverse modes coupling in higher harmonics of the cyclotron frequency [7]. However, analysis showed that a higher order axial mode of the bunching cavities, the TE_{112} mode at approximately 40.4 GHz, would be difficult to suppress. This mode could only be weakly cut off in the drift space separating the cavities because of the need to propagate the electron beam. As a result, the axial profile function of the TE_{112} mode extended substantially farther into the drift space than that of the TE_{111} mode, resulting in a substantially lower starting current. In order to further suppress the TE_{112} mode without loading down the TE_{111} mode excessively, additional pairs of 7.5–mm–long slots (see Fig. 2) were placed in the walls of the cutoff sections. These slots begin just beyond the main cavity slots, but are at an angle of 90° to them. The

combination of large slots at 90° intervals in different regions of the cutoff sections was intended to limit the axial extent of the rf fields of the TE_{112} mode of the cavity. They were also intended to substantially lower the Q of the TE_{11} mode of the drift spaces, of any polarization, as well as of other modes that might occur at higher harmonics of the cyclotron frequency, in order to prevent the build–up of oscillation in the drift spaces. The design of the entire rf circuit is discussed in detail by Fliflet *et al.* [7].

Despite these measures, an important limitation to the available parameter space of these gain measurements was the need to avoid exciting the TE_{112} mode. As predicted, too high a beam α, or too high a magnetic field, would cause this mode to oscillate during the flat portion of the VEBA voltage waveform, during which the amplification measurement at ~35 GHz must take place. The presence of this mode both at high α and at high magnetic field was verified by determining that an observed oscillating mode produced power that could propagate through a short section of V–band waveguide, with cutoff frequency of 40.0 GHz, but not through a section of W–band waveguide, with cutoff frequency of 59.35 GHz. Limiting operation to lower magnetic fields and lower beam α in order to avoid exciting this mode moved the 35 GHz operation to relatively large detunings and lower gains, compared to the optimum values predicted for this circuit by Fliflet *et al.* [7].

III. Theory

Early results on the small–signal theory of the gyroklystron were reported by Ergakov and Moiseev [12] and Symons and Jory [4]. A nonlinear analysis of the two–cavity gyroklystron has been given by Ganguly and Chu [13] and a small–signal, self–consistent field theory of the multicavity gyroklystron has been given by Ganguly, Fliflet and McCurdy [14]. A small–signal theory of the multicavity gyroklystron based on Gaussian axial profiles for the cavity electric fields and expressed in terms of

well–known gyrotron normalized parameters has been given by Tran *et al.* [15]. The theory of the phase–locked gyrotron with a prebunching cavity has been treated in the small–signal approximation, including finite temperature effects, by Manheimer [16], and in the nonlinear regime by Fliflet and Manheimer [17]. The theoretical approach given in Ref. [15] has been used to calculate the small–signal gain for the present configuration in the cold beam approximation. The phase bunching of the beam at the entrance to the second cavity is characterized by the bunching parameter:

$$q = \sqrt{\pi} F_1 \mu_1 e^{-(\mu_1 \Delta/4)^2} \left[\sqrt{3}\mu_1/2 + \mu_d \right] \tag{3}$$

where F_1, μ_1, and Δ are normalized peak electric field amplitude, interaction length, and resonance detuning parameters for the first cavity, and μ_d is the normalized length of the drift section. The normalized amplitude of the rf electric field induced in the second cavity by the phase–bunched beam is given by:

$$F_2 = \sqrt{\pi} I_2 \mu_2 e^{-(\mu_2 \Delta/4)^2} J_1(q) \left[\sin\psi + \frac{\mu_2^2 \Delta/4 - 1}{\sqrt{3}\mu_1/2 + \mu_d} \cos\psi \right] \tag{4}$$

where I_2 and μ_2 are the normalized current and length parameters for the second cavity, ψ is essentially the phase difference between the rf fields in the first and second cavities, and J_1 is a regular Bessel function of the first kind. For a linearly polarized TE_{1n} circular waveguide mode, an on–axis beam, and the fundamental harmonic interaction, the normalized quantities are defined according to:

$$I_i = \left[\frac{2}{\pi} \right]^{5/2} \frac{|e|\mu_0}{4 m_0 c} \frac{Q_i}{\gamma_0 \beta_{\perp 0}^4} \frac{\lambda}{d_i} \frac{1}{\left(x_i^2 - 1\right) J_1^2(x_i)} I_0 \tag{5}$$

$$\mu_i = \pi \frac{\beta_{\perp 0}^2}{\beta_{\parallel 0}} \frac{d_i}{\lambda} \tag{6}$$

$$\Delta = \frac{2}{\beta_{\perp 0}^2}\left(1 - \frac{\Omega}{\omega}\right) \tag{7}$$

$$F_i = \frac{2|e|}{m_0 c^2} \frac{r_{wi}}{\gamma_0 \beta_{\perp 0}^3 x_i} E_i \tag{8}$$

where the subscript i is the cavity index, e and m_0 are the electron charge and rest mass, μ_0 is the free–space permeability, c is the speed of light, x_i is a zero of J_1', λ is the free space wavelength, d_i is the effective interaction length, $\beta_{\perp 0}$ and $\beta_{\|0}$ are the average transverse and axial electron velocities normalized to c, γ_0 is the relativistic energy factor, Q_i is the cavity quality factor, r_{wi} is the cavity wall radius, E_i is the peak cavity rf field, I_0 is the beam current, Ω is the relativistic cyclotron frequency, and ω is the wave frequency. Except as noted, all quantities are expressed in MKS units. Equation (4) agrees with the result given in Ref. [15] except for the presence of the term proportional to $\cos\psi$. This term was not included in Ref. [15] or Ref. [7], which both assume operation at detunings (magnetic fields) for which $\mu^2\Delta/4 \approx 1$. This is a conventional choice for obtaining a high threshold current for self–oscillation of the bunching cavity, but unnecessarily restricts the generality of the result. The gain is calculated by relating F_2 to F_1 using Eqs. (3) and (4), and noting that the power generated by the second cavity (P_{out}) is related to the power injected into the first cavity (P_{in}) as:

$$P_{out} = P_{in} \frac{F_2^2 Q_{1int}}{F_1^2 Q_2} \tag{9}$$

Here Q_{1int} corresponds to the internal quality factor of the first cavity.

IV. Experimental Results

The principal measurements were a straightforward gain measurement and a frequency comparison between the first and second cavities. Measurements were carried out as a function of the drive frequency applied to the first cavity and as a function of experimental parameters. The diode voltage was 950±50 keV, the beam current was 150±20 A, and the calculated beam α was 0.36. The beam α was calculated using a fully relativistic single particle simulation that calculates electron particle trajectories in the combination of solenoidal fields and the fields due to the wiggler windings. The wiggler fields were calculated from a complete Biot–Savart solution of the fields due to a one–period untapered wiggler coil with realistic closures at each end.

The frequency of the second cavity was tracked by a heterodyne diagnostic as the driver magnetron frequency was varied. To do this, the signal from OUT–2 was split by a 3 dB coupler, and half of it was combined in a balanced mixer with a local oscillator (an IMPATT diode) whose frequency could be tuned separately from the frequency of the driver magnetron. Both the magnetron and the IMPATT frequencies were monitored by separate frequency meters whose relative calibration was determined by cold test. By this means, the difference frequency, Δf_0, between the drive signal and local oscillator signal could be determined for each separate experimental discharge. The experimental value of Δf for the output of the second bunching cavity, when the first bunching cavity was driven at a known frequency, was determined by analysis of the signal from the balanced mixer, which was recorded on an analog oscilloscope. The maxima and zero crossings of the mixer signal were used to count the full and fractional "beats" of the local oscillator frequency against the output frequency of the second cavity during a central 20 nsec central interval within the output pulse length. The number of cycles of the beat signal divided by the reference time interval yields an experimental measure of Δf.

Figure 3 shows a measurement of the variation of the second cavity output frequency as a function of the frequency of the driver magnetron, with the local oscillator frequency held fixed. This data was taken with a cavity magnetic field of 26.6 kG. The plot actually compares the measured beat frequency, Δf, between the local oscillator (at 35.23±.02 GHz) and the second cavity output frequency as the first cavity drive frequency was varied between 34.98 GHz and 35.27 GHz. The solid line indicates the predicted beat frequency, Δf_0. This data indicates that the frequency of the signal in the second bunching cavity tracks the drive frequency of the first bunching cavity, i.e., that the gyroklystron circuit is amplifying the signal injected into the first cavity. (In the absence of the beam, there is no measurable leakage between the two cavities at the drive frequencies.)

The amplification factor is measured by determining the ratio of the power generated in the second cavity, as monitored through the coupling port **IN–2** (see Fig. 1), to the power injected into the first cavity through the coupling port labeled **IN–1**, as monitored by the sampling port **OUT–1**. This determination depends sensitively on the calibration of the coupling factors of the various apertures on the first and second bunching cavities. The cold tests were carried out as follows: At critical coupling, essential all of the drive signal at the coupling aperture flows into the first cavity, and is dissipated in the other cavity losses, in this case dominated by the cavity slots. Cold tests were used to determine the ratio of the power injected into **IN–1** to the power detected at **OUT–1**. To determine the power generated in the second cavity, it was assumed that only 37% of the power was coupled out of port **IN–2**, while the remainder was delivered to the internal cavity losses, dominated by the cavity slots (see the discussion in Section II). Thus, the measured signal was multiplied by 2.7.

Figure 4 plots the linear gain between the first and second cavities as a function of the axial magnetic field at a drive frequency of 35.19 GHz, along with the

predicted gain. The experimental data were taken by varying the field provided by the cavity solenoid while keeping the main axial magnetic field fixed. Each point in the figure represents a single experimental discharge. The measured gain peaks in the vicinity of 28.5 kG. The highest single–discharge gain factor is ~90×, corresponding to a gain of approximately 19 dB. Based on the difficulty in calibrating the various cavity coupling factors, the uncertainty in this value is at least 3 dB. The highest second cavity powers were in the range of 50 to 100 kW, while typical first cavity drive powers were in the range of 1 to 2 kW.

The predicted gain shown in Fig. 4 is calculated from Eq. (9). It is found by optimizing Eq. (4) with respect to ψ, and assumes a 950 keV, 150 A, α=0.36 beam. In obtaining this curve, the Bessel function $J_1(q)$ in Eq. (4) was approximated by $q/2$. From approximately 22 to 28.5 kG, theory and experiment agree moderately well. The experiment actually does slightly better than the theoretical model in this range of magnetic fields. (It should be noted that small changes in the experimental values of current, voltage, magnetic field, and beam α could produce 50% changes in the predicted gain.) Theory shows the gain to continue to rise at higher magnetic fields, while the data show the gain rolling over. This is believed to be due to the onset of oscillation of the TE_{112} mode. Data taken at still higher magnetic fields show clear evidence of this oscillation. Thus, the substantially higher gains predicted at higher magnetic fields are inaccessible due to mode competition. Future efforts will concentrate on achieving stable operation of the third cavity (output cavity), and achieving stable three–cavity gyroklystron amplifier operation.

V. Discussion

We have carried out a fundamental–mode two–cavity K_a–band gyroklystron amplifier experiment driven by a 1 MeV, 150 A electron beam from a pulseline accelerator. We have demonstrated that the output frequency of the device tracks the

drive frequency, over the range from 35.0 to 35.3 GHz, and have found a regime of stable amplification, with a gain of up to 19 dB. This performance is in reasonable agreement with the predictions of theory. The peak output power of ~100 kW was limited by the available drive power, and did not correspond to saturation. The available parameter space for amplifier operation was limited by the excitation of parasitic oscillation of the competing TE_{112} mode, as predicted by theory [7]. Despite this limitation, these measurements have demonstrated the feasibility of operating gyroklystron amplifiers with megavolt electron beams. In addition, we have demonstrated the feasibility of using multiple bunching cavities to increase the rf fields available for beam bunching. The resulting increase in bunching would make possible higher gain in a gyroklystron amplifier, or a larger locking bandwidth in a gyroklystron oscillator.

Acknowledgments

The authors are grateful for useful discussions with Professor V.L. Granatstein and R. Fischer.

This work was supported by the Office of Naval Research.

References

1. A.C. England and H. Hsuan, "Electron Cyclotron Heating in Tokamaks and Tokamak Reactors," in *Wave Heating and Current Drive in Plasma*, edited by V.L. Granatstein and P.L. Colestock (Gordon and Beach, New York, 1985), pp. 459–509.

2. V.L. Granatstein, P. Vitello, K.R. Chu, K. Ko, P.E. Latham, W. Lawson, C.D. Striffler, and A. Drobot, "Design of gyrotron amplifiers for driving 1 TeV e^-e^+ linear colliders," *IEEE Trans. Nucl. Sci.*, vol. NS–32, pp. 2957–2959, 1985.

3. L.R. Barnett, L.H. Chang, H.Y. Chen, K.R. Chu, W.K. Lau, and C.C. Tu, "Absolute instability competition and suppression in a millimeter–wave gyrotron traveling–wave tube," *Phys. Rev. Lett.*, vol. 63, pp. 1062–1065, 1989.

4. R.S. Symons and H.R. Jory, "Cyclotron Resonance Devices," in *Advances in Electronics and Electron Physics, Vol. 55*, edited by L. Marton and C. Marton (Academic Press, New York, 1981), pp. 1–75.

5. W.M. Bollen, A.H. McCurdy, B. Arfin, R.K. Parker, and A.K. Ganguly, "Design and performance of a three–cavity gyroklystron amplifier," *IEEE Trans. Plasma Sci.*, vol. PS–13, pp. 417–423, 1985.

6. W.M. Black, S.H. Gold, A.W. Fliflet, D.A. Kirkpatrick, W.M. Manheimer, R.C. Lee, V.L. Granatstein, D.L. Hardesty, A.K. Kinkead, and M. Sucy, "Megavolt, multi–kiloamp K_a–band gyrotron oscillator experiment," *Phys. Fluids B*, vol. 2, pp. 193–198, 1990.

7. A.W. Fliflet, S.H. Gold, and W.M. Manheimer, "Design of a high voltage multi–cavity 35 GHz phase–locked gyrotron oscillator," *Int. J. Electron.*, vol. 67, pp. 111–130, 1989.

8. J.R. Bettis, J.K. Burton, R.K. Parker, S.H. Gold, M. Herndon, R.H. Jackson, A.K. Kinkead, A.H. Guenther, and E.J. Kobiela, "Laser–triggered switch modification to VEBA," *IEEE Trans. Nucl. Sci.*, vol. NS–28, pp. 3091–3093, 1981.

9. S.H. Gold, D.L. Hardesty, A.K. Kinkead, L.R. Barnett, and V.L. Granatstein, "A high–gain 35 GHz free–electron laser amplifier experiment," *Phys. Rev. Lett.*, vol. 52, pp. 1218–1221, 1984.

10. L. Friedland, "Electron beam dynamics in combined guide and pump magnetic fields for free electron laser applications," *Phys. Fluids*, vol. 23, pp. 2376–2382, 1980.

11. J.C. Slater, *Microwave Electronics* (Van Nostrand, New York, 1950), Chap. 5.

12. V.S. Ergakov and M.A. Moiseev, "Theory of synchronization of oscillations in a cyclotron–resonance maser monotron by an external signal," *Izv. Vyssh. Uchebn. Zaved., Radiofiz.*, vol. 18, pp. 120–131, 1975; also, *Radiophys. Quantum Electron.*, vol. 18, pp. 89–96, 1975.

13. A.K. Ganguly and K.R. Chu, "Analysis of two–cavity gyroklystron," *Int. J. Electron.*, vol. 51, pp. 503–520, 1981.

14. A.K. Ganguly, A.W. Fliflet, and A.H. McCurdy, "Theory of multicavity gyroklystron amplifier based on a Green's function approach," *IEEE Trans. Plasma Sci.*, vol. PS–13, pp. 409–416, 1985.

15. T.M. Tran, B.G. Danly, K.E. Kreischer, J.B. Schutkeker, and R.J. Temkin, "Optimization of gyroklystron efficiency," *Phys. Fluids*, vol. 29, pp. 1274–1281, 1986.

16. W.M. Manheimer, "Theory of the multi–cavity phase locked gyrotron oscillator," *Int. J. Electron.*, vol. 63, pp. 29–47, 1987

17. A.W. Fliflet and W.M. Manheimer, "Nonlinear theory of phase–locking gyrotron oscillators driven by an external signal," *Phys. Rev. A*, vol. 39, pp. 3432–3443, 1989.

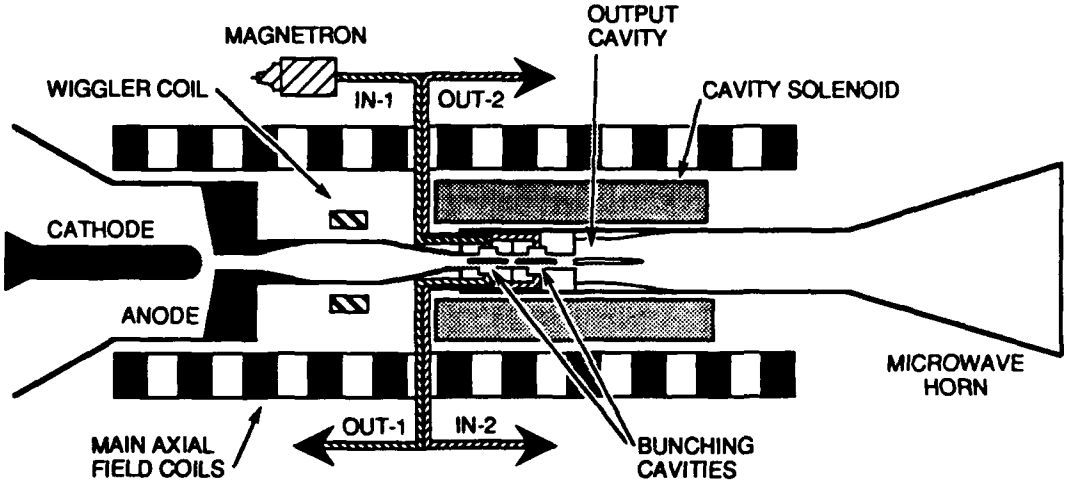

Fig.1. Schematic diagram of the gyroklystron experiment.

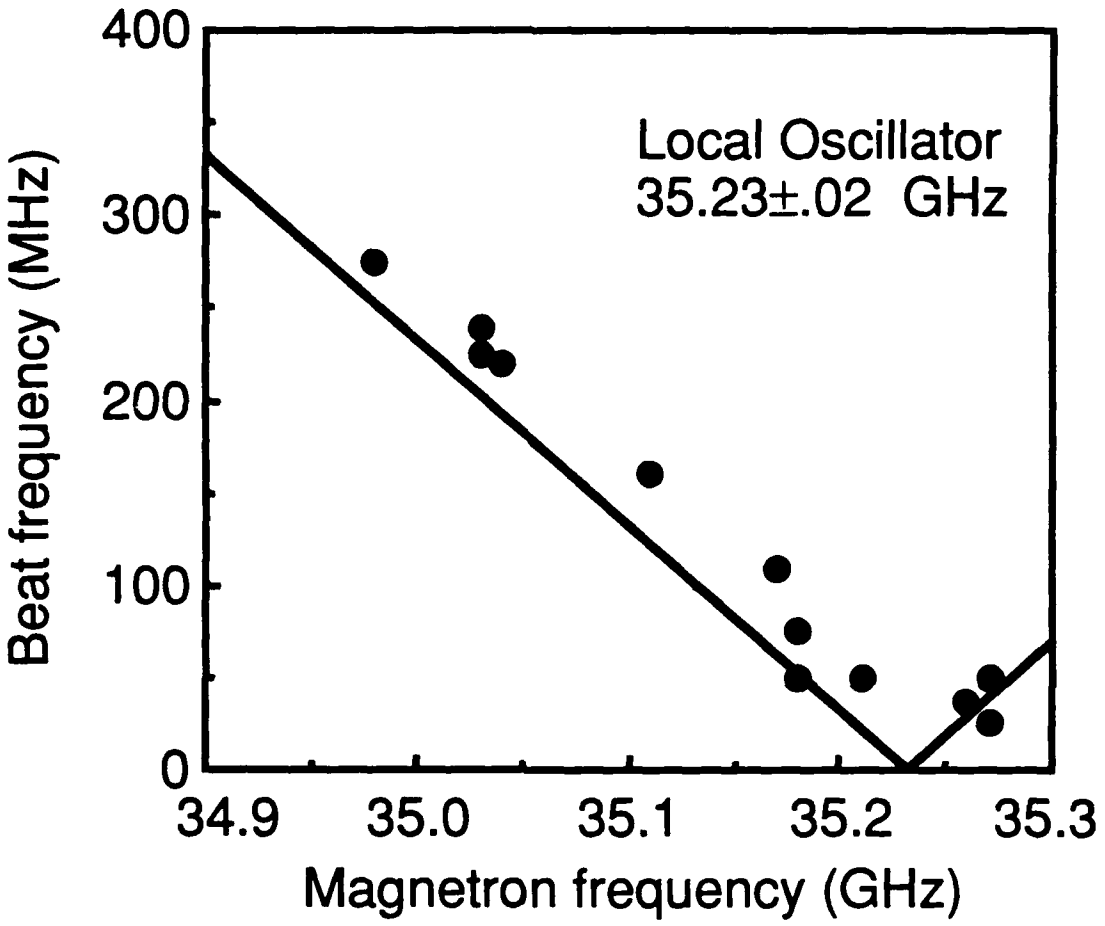

Fig. 3. Measured beat frequency between the local oscillator and the second cavity output frequency as a function of the drive frequency of the first cavity. The solid line is the calculated beat frequency based on the measured difference between the local oscillator and magnetron frequencies.

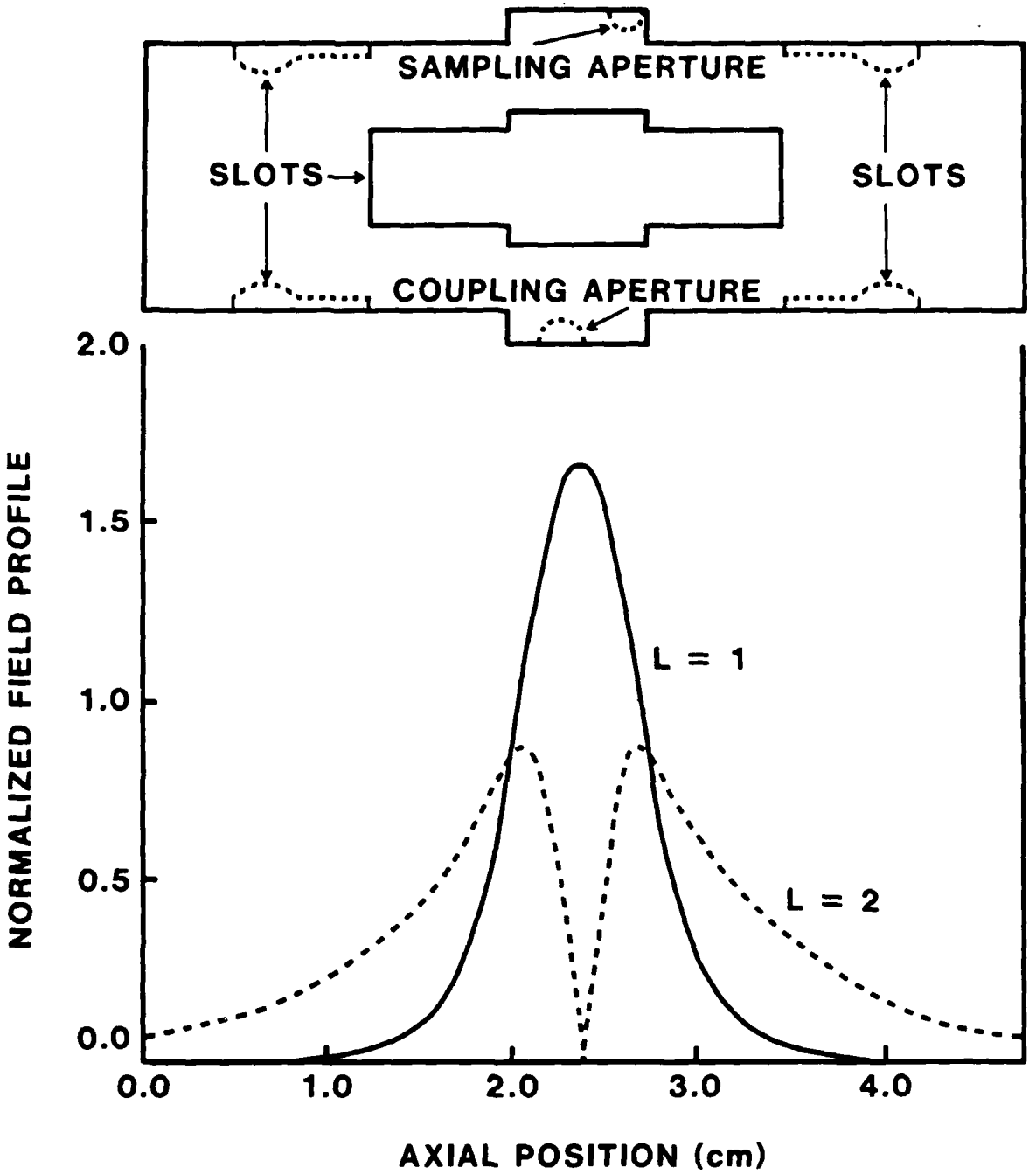

Fig. 2. Schematic of the bunching cavities, indicating the location of apertures and slots, and calculated axial profile functions for the TE_{111} and TE_{112} modes of the bunching cavities. (The calculated profiles do not include the effects of the four "keyhole" slots, which are expected to suppress the wings of the L=2 axial profile function.)

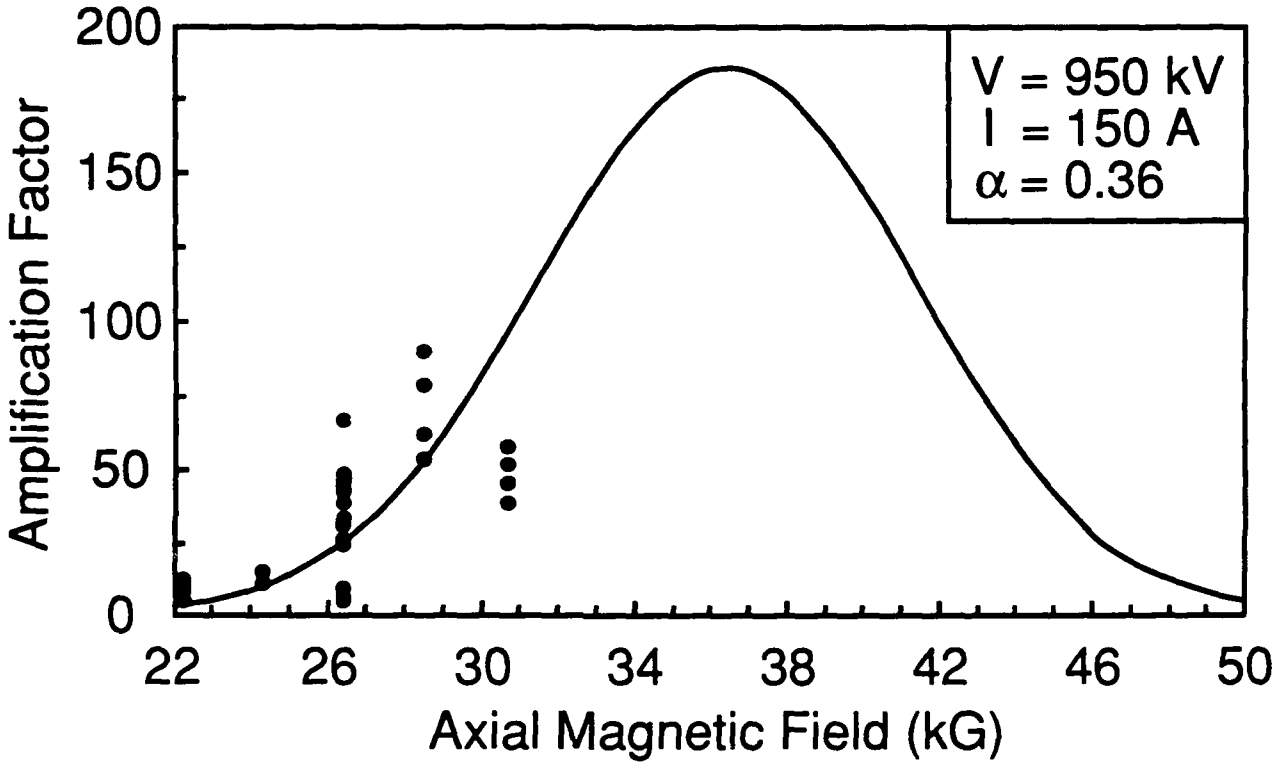

Fig. 4 Experimental power gain of the gyroklystron as a function of axial magnetic field. The solid line is the predicted gain, corresponding to a 950 keV, 150 A, α=0.36 beam.

4793/4 DISTRIBUTION LIST

Air Force Avionics Laboratory
AFWAL/AADM-1
Wright/Patterson AFB, OH 45433
Attn: Walter Friez — 1 copy

Air Force Office of Scientific Research
Bolling AFB
Washington, DC 20332
Attn: H. Schlossberg — 1 copy

Air Force Weapons Laboratory
Kirtland AFB
Albuquerque, NM 87117
Attn: Dr. W. Baker — 2 copies
Dr. A.H. Guenter — 1 copy

Columbia University
520 West 120th Street
Department of Electrical Engineering
New York, NY 10027
Attn: Dr. S.P. Schlesinger — 1 copy
Dr. A. Sen — 1 copy

Columbia University
520 West 120th Street
Department of Applied Physics
and Nuclear Engineering
New York, NY 10027
Attn: Dr. T.C. Marshall — 1 copy
Dr. R. Gross — 1 copy

Cornell University
School of Applied and Engineering Physics
Ithaca, NY 14853
Attn: Dr. H. Fleischmann — 1 copy
Dr. J. Nation — 1 copy
Dr. R.N. Sudan — 1 copy

Creol-FEL Research Pavillion
12424 Research Parkway, Suite 400
Orlando, FL 32826
Attn: Dr. L.R. Elias — 1 copy
Dr. I. Kimel — 1 copy

Dartmouth College
18 Wilder, Box 6127
Hanover, NH 03755
Attn: Dr. J.E. Walsh — 1 copy

Defense Advanced Research Project Agency, DEO
1400 Wilson Blvd.
Arlington, VA 22209
Attn: Dr. L. Buchanan — 1 copy

Defense Communications Agency
Washington, DC 20305
Attn: Dr. P.C. Jain,
Assistant for Communications Technology — 1 copy

Defense Nuclear Agency
Washington, DC 20305
Attn: Dr. L Wittwer (RAAE) — 5 copies

Defense Technical Information Center
Cameron Station
5010 Duke Street
Alexandria, VA 22314 — 2 copies

Department of Energy
Divison of Advanced Energy Projects
Washington, DC 20545
Attn: Dr. R. Gajewski — 1 copy

Department of Energy
Office of Energy Research
Washington, DC 20545
Attn: C. Finfgeld/ER–542, GTN — 1 copy
T.V. George/ER–531, GTN — 1 copy
D. Crandall/ER–54, GTN — 1 copy
Dr. David F. Sutter/ER–224, GTN — 1 copy

Director of Research
U.S. Naval Academy
Annapolis, MD 21402–5021 — 1 copy

General Atomics
13–260
Box 85608
San Diego, CA 92138
Attn: Dr. J. Doane — 1 copy
Dr. C. Moeller — 1 copy

Georgia Institute of Technology, EES–EOD
Baker Building
Atlanta, GA 30332
Attn: Dr. James J. Gallagher — 1 copy

Hanscomb Air Force Base
Stop 21, MA 01731
Attn: Lt. Rich Nielson/ESD/INK — 1 copy

Hughes Aircraft Co.
Electron Dynamics Division
3100 West Lomita Boulevard
Torrance, CA 90509
Attn: J. Christiansen — 1 copy
J. Tancredi — 1 copy

Hughes Research Laboratory
3011 Malibu Canyon Road
Malibu, CA 90265
Attn: Dr. R. Harvey — 1 copy
Dr. R.W. Schumacher — 1 copy

KMS Fusion, Inc.
3941 Resarch Park Dr.
P.O. Box 1567
Ann Arbor, MI 48106
Attn: S.B. Segall — 1 copy

Lawrence Berkeley Laboratory
University of California
1 Cyclotron Road
Berkeley, CA 94720
Attn: Dr. A.M. Sessler — 1 copy

Lawrence Livermore National Laboratory
P.O. Box 808
Livermore, CA 94550
Attn: Dr. D. Prosnitz — 1 copy
Dr. T.J. Orzechowski — 1 copy
Dr. J. Chase — 1 copy
Dr. W.A. Barletta — 1 copy
Dr. D.L. Birx — 1 copy
Dr. E.T. Scharlemann — 1 copy

Litton Electron Devices
960 Industrial Road
San Carlos, CA 94070
Attn: Library — 1 copy

Los Alamos National Laboratory
P.O. Box 1663, MSJ 564
Los Alamos, NM 87545
Attn: Dr. B. Newnam — 1 copy

Los Alamos National Laboratory
P.O. Box 1663, AT5-827
Los Alamos, NM 87545
Attn: Dr. T.J.T. Kwan — 1 copy
Dr. L. Thode — 1 copy
Dr. R.R. Bartsch — 1 copy

Massachusetts Institute of Technology
Department of Physics
Cambridge, MA 02139
Attn: Dr. G. Bekefi/36–213 — 1 copy
Dr. M. Porkolab/NW 36–213 — 1 copy
Dr. R. Davidson/NW 16–206 — 1 copy
Dr. A. Bers/NW 38–260 — 1 copy
Dr. K. Kreischer — 1 copy
Dr. B. Danly — 1 copy
Dr. G.L. Johnston — 1 copy

Massachusetts Institute of Technology
167 Albany St., N.W. 16–200
Cambridge, MA 02139
Attn: Dr. R. Temkin/NW 14–4107 — 1 copy

Mission Research Corporation
8560 Cinderbed Road, Suite 700
Newington, VA 22122
Attn: Dr. M. Bollen — 1 copy
Dr. J. Pasour — 1 copy

Naval Research Laboratory
Addressee: Attn: Name/Code
Code 0124 – ONR — 1 copy
Code 1000 – Commanding Officer — 1 copy
Code 1001 – T. Coffey — 1 copy
Code 1003.9A – Computer Resources Architect — 1 copy
Code 1005 – Head, Office of Mgt. and Admin. — 1 copy
Code 1005.1 – Deputy Head, Off. of Mgt. and Admin. — 1 copy
Code 1005.6 – Head, Directives Staff — 1 copy
Code 1200 – Capt. R.W. Michaux — 1 copy
Code 1201 – Deputy Head, Command Support Division — 1 copy
Code 1220 – Security — 1 copy
Code 2000 – J. Brown — 1 copy
Code 2604 – NRL Historian — 1 copy
Code 2628 – TID Distribution — 22 copy

Code 2634 – Cindy Sims	1 copy
Code 3000 – R. Doak	1 copy
Code 4000 – R. Ellis	1 copy
Code 4600 – D. Nagel	1 copy
Code 4700 – S. Ossakow	26 copy
Cope 4700.1 – A. Ali	1 copy
Code 4707 – W. Manheimer	1 copy
Code 4770 – G. Cooperstein	1 copy
Code 4790 – Branch Office	25 copy
Code 4790 – W.M. Black	1 copy
Code 4790 – A.W. Fliflet	1 copy
Code 4790 – S.H. Gold	1 copy
Code 4790 – T. Hargreaves	1 copy
Code 4790 – C. Hui	1 copy
Code 4790 – C. Kapetanakos	1 copy
Code 4790 – A.K. Kinkead	1 copy
Code 4790 – Y.Y. Lau	1 copy
Code 4790 – M. Rhinewine	1 copy
Code 4790 – P. Sprangle	1 copy
Code 5700 – L. Cosby	1 copy
Code 6840 – S. Ahn	1 copy
Code 6840 – C. Armstrong	1 copy
Code 6840 – A. Ganguly	1 copy
Code 6840 – R. Parker	1 copy
Code 6840 – N. Vanderplaats	1 copy
Code 6850 – L. Whicker	1 copy
Code 6875 – R. Wagner	1 copy

Naval Sea Systems Command
Department of the Navy
Washington, DC 20362
Attn: Commander, PMS 405–300 — 1 copy

Northrop Corporation
Defense Systems Division
600 Hicks Rd.
Rolling Meadows, IL 60008
Attn: Dr. Gunter Dohler — 1 copy

Oak Ridge National Laboratory
P.O. Box Y
Mail Stop 3
Building 9201–2
Oak Ridge, TN 37830
Attn: Dr. A. England — 1 copy

Office of Naval Research
800 N. Quincy Street
Arlington, VA 232217
Attn: Dr. C. Roberson — 1 copy

Office of Naval Research
1012 W. 36th Street, Childs Way Bldg.
Los Angeles, CA 90089–1022
Attn: Dr. R. Behringer — 1 copy

Optical Scines Center
University of Arizona
Tuscon, AZ 85721
Attn: Dr. Willis E. Lamb, Jr. — 1 copy

Physical Sciences Inc.
603 King Street
Alexandria, VA 22314
Attn: M. Read — 1 copy

Physics International
2700 Merced Street
San Leandro, CA 94577
Attn: Dr. J. Benford — 1 copy

Princeton Plasma Physics Laboratory
James Forrestal Campus
P.O. Box 451
Princeton, NJ 08544
Attn: Dr. H. Hsuan — 1 copy
Dr. D. Ignat — 1 copy
Dr. H. Furth — 1 copy
Dr. P. Efthimion — 1 copy
Dr. F. Perkins — 1 copy

Raytheon Company
Microwave Powrer Tube Division
Foundary Avenue
Waltham, MA 02154
Attn: N. Dionne — 1 copy

Sandia National Laboratory
Org. 1231, P.O. Box 5800
Albuquerque, NM 87185
Attn: Dr. Thomas P. Wright — 1 copy
Mr. J.E. Powell — 1 copy
Dr. J. Hoffman — 1 copy
Dr. W.P. Ballard — 1 copy
Dr. C. Clark — 1 copy

Science Applications International Corp.
1710 Goodridge Dr.
McLean, VA 22102
Attn: Dr. A. Drobot — 1 copy
Dr. P. Vitello — 1 copy
Dr. D. Bacon — 1 copy
Dr. C. Menyuk — 1 copy

Science Research Laboratory
15 Ward Street
Somerville, MA 02143
Attn: Dr. R. Shefer — 1 copy

SPAWAR
Washington, D.C. 20363
Attn: E. Warden, Code PDE 106–3113 — 1 copy
Capt. Fontana — 1 copy

Spectra Technologies
2755 Northup Way
Bellevue, WA 98004
Attn: Dr. J.M. Slater — 1 copy

Stanford University
Department of Electrical Engineering
Stanford, CA 94305
Attn: Dr. J. Feinstein — 1 copy

Standford University
High Energy Physics Laboratory
Stanford, CA 94305
Attn: Dr. T.I. Smith — 1 copy

Stanford University
SLAC
Stanford, CA 94305
Attn: Dr. Jean Labacqz — 1 copy

TRW, Inc.
One Space Park
Redondo Beach, CA 90278
Attn: Dr. H. Boehmer — 1 copy
Dr. T. Romisser — 1 copy
Dr. Z. Guiragossian — 1 copy

University of California
Physics Department
Irvine, CA 92717
Attn: Dr. G. Benford — 1 copy
Dr. N. Rostoker — 1 copy

University of California
Department of Physics
Los Angeles, CA 90024
Attn: Dr. A.T. Lin — 1 copy
Dr. N. Luhmann — 1 copy
Dr. D. McDermott — 1 copy

University of Maryland
Department of Electrical Engineering
College Park, MD 20742
Attn: Dr. V.L. Granatstein — 1 copy
Dr. W.W. Destler — 1 copy

University of Maryland
Laboratory for Plasma and Fusion Energy Studies
College Park, MD 20742
Attn: Dr. Tom Antonsen — 1 copy
Dr. John Finn — 1 copy
Dr. Jhan Varyan Hellman — 1 copy
Dr. W. Lawson — 1 copy
Dr. Baruch Levush — 1 copy
Dr. Edward Ott — 1 copy
Dr. M. Reiser — 1 copy

University of New Mexico
Department of Physics and Astronomy
800 Yale Blvd., N.E.
Albuquerque, NM 87131
Attn: Dr. Gerald T. Moore — 1 copy

University of Tennessee
Department of Electrical Engineering
Knoxville, TN 37916
Attn: Dr. I. Alexeff — 1 copy

University of Utah
Department of Electrical Engineering
3053 Merrill Engineering Bldg.
Salt Lake City, UT 84112
Attn: Dr. Larry Barnett — 1 copy
Dr. J. Mark Baird — 1 copy

U.S. Army
Harry Diamond Laboratories
2800 Powder Mill Road
Adelphi, MD 20783–1145
Attn: Dr. H. Brandt — 1 copy
Dr. E. Brown — 1 copy
Dr. S. Graybill — 1 copy
Dr. A. Kehs — 1 copy
Dr. J. Silverstein — 1 copy

Varian Associates
611 Hansen Way
Palo Alto, CA 94303
Attn: Dr. H. Huey — 1 copy
Dr. H. Jory — 1 copy
Dr. K. Felch — 1 copy
Dr. R. Pendleton — 1 copy
Dr. A. Salop — 1 copy

Varian Eimac San Carlos Division
301 Industrial Way
San Carlos, CA 94070
Attn: Dr. C. Marshall Loring — 1 copy

WL/CA
Kirtland AFB, NM 87117–6008
Attn: Dr. Brendan B. Godfrey — 1 copy

Yale University
Department of Applied Physics
Madison Laboratory
P.O. Box 2159
Yale Station
New Haven, CT 06520
Attn: Dr. I. Bernstein — 1 copy

Naval Research Laboratory
Washington, DC 20375-5000
Code 4830
Tim Calderwood — 1 copy

Records — 1 copy